PCCP

Accepted Manuscript

ROYAL SOCIETY OF CHEMISTRY

www.rsc.org/pccp

Structure of ionic liquid/water mixtures investigated by IR and NMR spectroscopy

Seoncheol Cha[1**], Mingqi Ao[1**], Woongmo Sung[1], Bongjin Moon[2], Bodil Ahlström[3], Patrik Johansson[3], Yukio Ouchi[4], and Doseok Kim[1]*

1) Department of Physics, Sogang University, Seoul 121-742 Korea

2) Department of Chemistry, Sogang University, Seoul 121-742 Korea

3) Department of Applied Physics, Chalmers University of Technology, SE-412 96 Göteborg, Sweden

4) Department of Organic and Polymeric Materials, Tokyo Institute of Technology, Tokyo 152-8552 Japan

*Corresponding author: doseok@sogang.ac.kr

** These authors contributed equally to this work.

Abstract

Imidazolium-based ionic liquids having different anions (1-butyl-3-methylimidazolium ([BMIM]X: X = Cl^-, Br^-, I^-, and BF_4^-) and their aqueous mixtures were investigated by IR absorption and proton NMR spectroscopy. The IR spectra of these ionic liquids in the CH_x stretching region differed substantially, especially for C-H bonds in the imidazolium ring, and the NMR chemical shifts of protons in the imidazolium ring also varied markedly for ILs having different anions. With the introduction of water to screen the electrostatic forces and separate the ions, both IR and NMR spectra of [BMIM]X (X = Cl^-, Br^-, I^-) showed significant changes, while those for $[BMIM]BF_4$ did not change appreciably. H-D isotopic exchange rates of C(2)-H in $[BMIM]X/D_2O$ mixtures exhibited an order: C(2)-H···Cl > C(2)-H···Br > C(2)-H···I, while the C(2)-H of $[BMIM]BF_4$ was not deuterated at all. These experimental findings, supported by DFT calculations, lead to the microscopic bulk configurations in which the anions and the protons of the cations in the halide ionic liquids have specific, hydrogen-bond type of interaction, while the BF_4^- anion does not participate in the specific interaction, but interacts less specifically by positioning itself more above the ring plane of the imidazolium cation. This structural change dictated by the anion type will work as a key element to build the structure-property relation of ionic liquids.

1. Introduction

Ionic liquids (ILs) are a class of novel compounds composed exclusively of cations and anions that exist in the liquid state below 100 °C. They have attracted considerable interest due to their unique appealing features, such as low melting points, negligible vapor pressure, chemical stability, and wide electrochemical windows[1,2]. These properties suggest that ILs might potentially be 'green' alternatives to conventional organic solvents[3–5]. Thus, particular efforts have been devoted to understand the microscopic intermolecular structure of ILs[6–11], as it determines key properties of ILs such as density, viscosity, surface tension, ionic conductivity, heat capacity, and solubility. Thus, many studies using different methods have been reported to unveil the microscopic bulk structures of ILs. Simulations have proposed how the microscopic configurations like relative position may change by the change of cation or anion[12,13]. A role played by the alkyl chain attached to the cation of the prototype ILs having 1-alkyl-3-methylimidazolium cation ($[C_nMIM]^+$) has been suggested[14,15]. Unique microdomain structure consisting of polar and non-polar moieties of the IL proposed from X-ray and neutron scattering studies[16–18] was borne out by molecular dynamics (MD) simulations[19,20]. Spectroscopic techniques in the low-frequency range, suited to probe intermolecular or interionic interactions, have been used to study the spectral features changing with the type of cation or anion [21–23].

For prototypical imidazolium-based ILs, hydrogen bonding between the cation and anion has been regarded crucial in determining the microscopic structures and macroscopic properties. For example, Hunt used density functional theory (DFT) calculations to explain the relation between viscosity and hydrogen bonding in ILs[24]. Fumino et al. studied the effect of hydrogen bonding on bulk properties, such as melting point and viscosity of ILs using poly-methylated imidazolium-based cations and bis(trifluoromethylsulfonyl)imide (NTf_2) anion using far-IR, and terahertz spectroscopy[25]. The role of hydrogen bonding in the crystal structure was also investigated[26].

Due to its importance on the IL properties and structures, there have been many studies on the ion-species dependence on the hydrogen bonding strength[27–30]. Dong et al. obtained the optimized geometry of imidazolium-based ILs having different anions to predict the hydrogen-bonded ion pairs by density functional theory (DFT) calculations[28]. Ludwig group found the bond strength change for different cations and anions using far-IR spectroscopy and DFT calculations.[29,30] , and Gao et al. made the order of hydrogen bonding strength for ILs having different anions[27]. Even for pure ILs, however, e.g. the spectroscopic assignments in the C-H stretching region can be very complicated, as shown by the detailed studies employing both IR and Raman spectroscopy as well as anharmonic DFT frequency calculations[31–33]. These studies show the presence and importance of Fermi resonances (FR) and overtones coupled to the imidazolium ring vibrations in this region, unfortunately making any unambiguous comparison across a full set of ILs impossible. Earlier spectroscopic work on ILs not taking this aspect into account should thus be used with due care.

DFT calculations and ab initio MD simulations found that the IR vibrational frequency and NMR chemical shift of C(2)-H were excellent indicators of the relative strength of hydrogen bonding[34–37], while this strength could be reduced in IL/solvent mixtures by the screening effect of solvent molecules. For this reason, monitoring IL/solvent mixtures by IR and NMR spectroscopy has been fruitful, and the existence of specific, strong hydrogen bonding in the strongly coordinated ILs, such as halide anions having large electronegativity was measured by this technique[38,39]. However, the nature and the strength of interaction in the weakly coordinated ILs, such as $[C_nMIM]BF_4$, is still debated. The C(2)-H and F cross peak of hetero Nuclear Overhauser Enhancements (NOE) and spin-lattice relaxation time of C(2) carbon in NMR experiments suggested the C-H···F interaction between imidazolium cation and BF_4^- anion[40,41]. Zhang et al. observed the C(2)-H peak change of 1-ethyl-3-methylimidazolium tetrafluoroborate ($[EMIM]BF_4$)/water mixtures to propose the existence of the hydrogen bonding between cation and BF_4^-[42]. By contrast, other groups reported that the IR spectra of $[C_nMIM]BF_4$ dissolved in the acetone or water did not change remarkably, to support the nonspecific interaction between cation and BF_4^-[43–45].

In addition to studying the interaction between cation and anion, the interactions between ions and solvents were also studied for different organic solvents, such as dimethyl sulfoxide and acetonitrile[46,47]. Wang et al. studied pyridinium-based ILs to compare them with the imidazolium-based ILs by IR spectroscopy and DFT calculations, and solvent mixtures with ILs having different anions were also investigated[48–50]. Various experimental techniques are applied to study the IL/solvent mixtures. The libration and translation motions of water in imidazolium-based ILs measured by far-IR spectroscopy was observed, to suggest hydrogen bonding between BF_4^- and water, but not between PF_6^- and water[51]. Terahertz and optical Kerr effect (OKE) spectroscopy were used to study the mixture of [BMIM]BF_4 with water and acetonitrile[23,52,53]. The phase diagram of ionic liquids with organic solvent was determined experimentally[54]. . Large-Angle X-ray scattering was applied to study the interaction in ILs by measuring the structure functions of [EMIM]BF_4/water mixtures[45].

Several MD simulations results are reported on IL/solvent mixtures that investigated the interaction between ions and solvent molecules. Moreno et al. studied [BMIM]BF_4/water mixture by MD to compare with the NMR data, and found the short range IL/water interactions at low water concentrations and the nonselective interaction at high water concentrations[55]. Porter et al. compared the effect of small amount of water for water-miscible and immiscible ILs by using MD simulations, and found the existence of hydrogen bonding between anion and water as well as dramatic change of self-diffusion coefficients due to the water[56]. Chang et al. performed the MD simulations on the N,N-diethyl-N-methylammonium triflate([DEMA]Tfl)/water mixture and found the weakening of ions association and the enhancement of translational and rotational motion of ions by adding the water molecules[7].

To investigate the relation between cation-anion interaction and the microscopic bulk structures, ILs having halide anions are a good starting point; by changing the anion following down the periodic table the interaction can be varied systematically. The fundamental understanding built up from studying these simple anions can later be applied when the constituent cations and anions are changed into more complex ions. Here we choose to study

halide ILs having the prototypical cation 1-butyl-3-methylimidazolium ([BMIM]X, X = Cl^-, Br^-, I^-) together with $[BMIM]BF_4$, in pure form and aqueous solution, to observe how the change of anion alters the interionic interactions and the bulk structure of these otherwise similar ILs. By varying the concentration of ILs in water, it can be envisaged that the interionic interaction gets screened very effectively, and thus the distance between the cation and the anion continuously changes – until isolated cations and anions are obtained in very dilute systems.

IR spectroscopy and nuclear magnetic resonance (NMR) were the tools chosen to investigate these ILs. IR spectroscopy has been commonly used as an analytical tool to identify intra-molecular vibrational normal modes; recently it was found that the strength of hydrogen bonding between the cation and anion in ILs is reflected sensitively in the spectrum to allow investigation of intermolecular interactions and conformations[34,44,50,57–60]. NMR is also a useful tool to investigate the nature of interaction between the cation and the anion, or between the solvent molecules and the IL species in solution[11,40,61–64]. NMR has been used to study dynamics and relaxation processes in ILs[62–65], and 2D-NMR has been applied to investigate intermolecular interactions and nano-scale aggregates[40].

There have been many previous reports that investigated the structures of ionic liquids, but for most of these studies limited scope either in terms of the species investigated or techniques employed prevented comprehensive and deeper understanding of the structure. In this report, IR and NMR spectroscopy together with ab-initio calculations have been applied to study both pure ILs and aqueous solutions of [BMIM]X (X = Cl^-, Br^-, I^-) by systematic change of anions to investigate the interionic interactions in detail. The spectra obtained for $[BMIM]BF_4$ are also investigated to compare the single-atom anions with molecular anion. The change of the anion in the IL is readily reflected in the resulting spectra, and the analysis of the spectra from pure ILs together with their changes upon dilution allow us to propose detailed microscopic structures of these ILs.

2. Experimental and Computational Section

The tetrafluoroborate salt of 1-butyl-3-methyl imidazolium ([BMIM]BF_4), and the halide salts of 1-butyl-3-methyl imidazolium ([BMIM]Cl, [BMIM]Br, [BMIM]I) were purchased from C-TRI in Korea. The purity was higher than 99 wt% (water content < 170 ppm), and all were used without further purification. To check for the effect of this trace amount of water, an extra drying procedure was performed in a vacuum chamber with phosphorus pentoxide as drying agent for more than 1 day, which resulted in <10 ppm water content, as confirmed by Karl Fischer titration. Reassuringly, the IR spectra hardly changed compared to those of the as-received IL samples (except for the complete elimination of the weak OH band from 3200 – 3500 cm^{-1}). The NMR spectra were also identical before- and after the drying procedure. [BMIM]BF_4 and [BMIM]I are liquids at room temperature (thus room-temperature ILs), while both [BMIM]Br and [BMIM]Cl are solids. Therefore, the solid ILs were first melted at ~ 350 K on a hot plate, afterwards they remained in a supercooled liquid state at room temperature. All the aqueous solutions were prepared in D_2O (from Aldrich). For the Attenuated Total Reflection-Infrared (ATR-IR) spectroscopic measurements on aqueous solutions, the spectra were taken quickly after the solutions were made, to prevent any isotopic substitution of the hydrogen atoms in the imidazolium cation. Over time C(2)-H was selectively substituted into C(2)-D, and this was utilized to get $[BMIM]^+$ cation with C(2)-D, of which the IR spectrum was taken after drying to remove D_2O[32,66]. During the H-D exchange studies, we controlled the pH to 7 using a sodium phosphate buffer. The chemical structure of the $[BMIM]^+$ cation is shown in the inset of Fig. 1.

The ATR-IR spectra of the ILs and IL/water mixtures were collected from 650 to 4000 cm^{-1}. The resolution was 4 cm^{-1} and 256 scans were averaged for each spectrum. Proton NMR measurements were performed with a Varian Gemini 400 NMR spectrometer. An external double-reference method was used; the IL sample was transferred to an external tube, and a

2-mm coaxial insert NMR tube was filled with tetramethylsilane (TMS) in $CDCl_3$ as internal chemical shift references. For the deuteration studies the disappearance of the C(2)-H peak via the decrease in the peak area ratio between C(2)-H and C(4)-H was monitored. All the spectra were collected at room temperature.

The Density Functional Theory (DFT) calculations used two starting configurations, AA (two anti-conformations for the butyl chain) and GA (gauche conformation for the C-C bond closest to the imidazolium ring), for the isolated $[BMIM]^+$ cation[57], as well as for the corresponding ion-pair models for [BMIM]X (X = Cl^-, Br^-) and $[BMIM]BF_4$. Both IR data (vibrational frequencies and IR intensities calculated by analytical 2nd derivatives) and NMR data (using the GIAO method and the chemical shifts given relative to TMS) were calculated in gas phase and in addition for a simulated water environment using a continuum model (C-PCM, conductor-like polarizable continuum model with ε = 78.3553, standard value of water in Gaussian09) [67] All calculations were performed at the B3LYP/6-311+G* level of theory as implemented in Gaussian 03 [68].

3. Results and Discussion

3.1 Pure ionic liquids: IR spectra

Figure 1 shows the ATR-IR spectra in the 2800 — 3200 cm^{-1} CH_x stretching region for the pure ILs. Easily noticeable are the differences in the absorption strength by more than a threefold, as well as the overall spectral shape, especially distinguishing the $[BMIM]BF_4$ spectrum from the others. As these ILs all share the common $[BMIM]^+$ cation where the CH_x resides structurally, the large differences in the IR spectra are unusual and intriguing. To check for effects like probing depth change arising from differences in refractive indices, IR spectra were also measured in transmission (not shown), but yielded very similar results as in Fig. 1. As Cl^- is the smallest anion, the observed increase in absorbance of [BMIM]Cl could in principle also be due to the slight increase in cation number density, but the change is only

~0.1 %, far too small to account for the observed intensity change.

Another notable feature is an overall red-shift of the absorption bands from [BMIM]BF_4 to [BMIM]Cl, especially for those above 3000 cm^{-1}. We followed the previously assigned peak positions for [BMIM]BF_4 and [BMIM]I, and slightly shifted for C(2,4,5)-H peaks of [BMIM]Br and [BMIM]Cl from those of [BMIM]I by using least-square fitting.[66,69,70]. Figure 2 shows the decomposition of the spectra using multi-peak Gaussians, and the fitting parameters are to be found in Table 1. The peaks in the range from 2800 to 3000 cm^{-1} originate from the CH_x stretch vibrations of the butyl chain and the methyl group attached to the imidazolium ring. For [BMIM]BF_4, peaks at 2856, 2877, 2913, 2938 and 2965 cm^{-1} are attributed to the modes of $\nu_{ss}CH_2$, $\nu_{ss}CH_3$, $\nu_{as}CH_2$, $\nu_{FR}CH_3$ and $\nu_{as}CH_3$, respectively (ss, as, and FR represent the symmetric stretch, the antisymmetric stretch, and the Fermi resonance, respectively)[70,71]. For ILs based on halide anions, the above bands are slightly red-shifted from those of [BMIM]BF_4 as reported earlier[31,33,66,72].

The features above 3000 cm^{-1} arise from the CH_x stretching vibrational modes from the imidazolium ring. Here the spectrum of [BMIM]BF_4 differs markedly from the other ILs' spectra. The spectra of ILs with halides have redshifts and increased absorption in this range; in detail a gradual red-shift of the band around 3050 cm^{-1} can be seen from [BMIM]I to [BMIM]Cl. We started from the assignment of the C(2)-H mode (3018 – 3032 cm^{-1} for halides, and 3114 cm^{-1} for [BMIM]BF_4), which is made certain by selective deuteration of this hydrogen (Fig. 3, discussed more in section 3.5) [44]. The two modes at higher frequencies were assigned to ν_{as}(C(4,5)-H) and ν_{ss}(C(4,5)-H) [44]. From the spectra as well as from Table 1, the C(2)-H mode of ionic liquids having halide anions is visually red-shifted by as much as ~100 cm^{-1} from that of [BMIM]BF_4. Peak strengths also change considerably between [BMIM]BF_4 and the halide salts such that C(2)-H mode is much stronger for [BMIM]X (X = Cl^-, Br^-, I^-) as compared to that of [BMIM]BF_4. This demonstrates that the interaction between BF_4^- and imidazolium ring is totally different from those in the halide anions, while the difference is relatively minor between Cl^-, Br^-, and I^-. Note the complications and possible spectroscopic

difference enhanced by the presence of Fermi resonances (FR) and overtones, as previously mentioned[31-33].

The C(2)-H group holds the most acidic hydrogen atom in the cation owing to the electron deficit to the C=N π bond[58,59]. The red-shift of the ν(C(2)-H) band from [BMIM]I to [BMIM]Cl, suggests an interaction strength change. This can be identified more clearly from the C(2)-D stretching bands of the deuterated samples. Figure 3 shows the ATR-IR spectra of [BMIM]X with and without isotopic substitution of C(2)-H. These deuterated samples, by isotopic substituted imidazolium cations (d-[BMIM]), were decisive in the assignment of the CH-bands in the IR spectra. The decreased absorption in the band around 3000 cm^{-1} (~3010 cm^{-1} for [BMIM]Cl and [BMIM]Br, and 3024 cm^{-1} for [BMIM]I) is solely due to the deuteration of C(2)-H, as also confirmed by the NMR spectra (later section). The in-plane ring modes hardly changed between these three ILs before (~1570 cm^{-1}) and after (~1540 cm^{-1}) the isotopic substation, consistent with a previous report[32]. The deuterated ν(C(2)-D) stretch mode frequencies follow the same sequence: ~2275 cm^{-1} for chloride, ~2281 cm^{-1} for bromide, and ~2307 cm^{-1} for iodide anions. The C-H···anion hydrogen bonds in ILs have been termed red-shifted H-bonds[59,73], for which the red-shift of the C-H stretch vibration mode is an indicator of the weakening of these bonds[34], concurrent with the strengthening of hydrogen bond interactions with the proton acceptors. Thus an observed blue-shift of C(2)-H from [BMIM]Cl to [BMIM]I implies that the hydrogen bonds weaken in that order. In contrast, ν(C(2)-H) for [BMIM]BF_4 is found at 3114 cm^{-1}, ~100 cm^{-1} blue-shifted from those of halide based ILs, and does not change even for very dilute solutions, where the anion is not expected to have significant influence as reported previously[44,45]. Thus, this confirms that the hydrogen bonding within the [BMIM]BF_4 IL is much weaker as compared to ILs having halide anions.

From the DFT calculations using ion-pairs and isolated ions in Table 2, the C(2)-H peak is shown to blue-shift from [BMIM]Cl to [BMIM]BF_4 by as much as 500 cm^{-1}. Although the calculations follow the trend from the experimental results, we find that it is very difficult to extract quantitative information in this region as the effects of FR and decreasing ν(C(2)-H)

interactions are strongly mixed. However, for the series of ILs here investigated the DFT computed total ion-ion interaction energy, where the hydrogen bonding strongly contributes for the halide based ILs, decreases as expected; $\Delta E_{BMIM\text{-}Cl}$ = -374 kJmol^{-1}, $\Delta E_{BMIM\text{-}Br}$ = -355 kJmol^{-1}, and $\Delta E_{BMIM\text{-}BF4}$ = -346 kJmol^{-1} [57].

3.2 Pure ionic liquids: NMR chemical shifts

The experimental chemical shifts (δ) for all the protons of the [BMIM]$^+$ cation for all ILs are plotted in Fig. 4. Two factors have been known to contribute to the chemical shift[74]; hydrogen bonding with the anion and the inductive effect of its proximity to the imidazolium ring. Regardless of the anion type the C(2)-H proton showed the largest chemical shift, with the experimental values 10.22, 9.78, and 9.28 ppm for [BMIM]Cl, [BMIM]Br and [BMIM]I, respectively. This order works as an indicator of the hydrogen bonding strength of C(2)-H···Cl > C(2)-H···Br > C(2)-H···I. Shukla et al.[34] have investigated the strength of this type of H-bonding interaction between C(2)-H and halide anion by DFT calculations, and suggested structures possibly accountable for our materials. Following the electronegativity order (Cl^-: 3.0, Br^-: 2.8, and I^-: 2.5)[75], the C(2)-H···X distance was shown to increase gradually from Cl^- to I^-, and the average N(1)-C(2)-H-X dihedral angle to increase from C(2)-H···Cl to C(2)-H···I, both indicative of a weakened hydrogen bonding.

Computational studies using cluster and polarizable continuum models[76] indicate that the chemical downfield shift of the acidic protons of the aromatic ring is mainly caused by hydrogen bonding interaction[74]. Our present computations, keeping in mind recent observations on how to accurately predict ^{1}H NMR shifts of ILs by DFT calculations[35], are consistent with these observations – the relative shift of the C(2)-H proton being affected the most upon formation of ion-pair as compared to isolated [BMIM]$^+$ IL cation. The computed values for the C(2)-H proton are 7.6 ppm (isolated [BMIM]$^+$) as compared to 14.5 ppm ([BMIM]Br) and 14.8 ppm ([BMIM]Cl). The experimental difference between the Cl and Br anion (~0.44 ppm) is rather well mimicked by this model (~0.3 ppm), especially when

considering this simple DFT approach. As a comparison the [BMIM]BF_4 ion-pair results in 10.0 ppm, thus indicating the sequence of the hydrogen bonding strength as C(2)-H···Cl > C(2)-H···Br > C(2)-H···BF_4, in qualitative agreement with the experimental result in Fig. 4. All other protons show significantly smaller shifts upon ion-pair formation compared to the isolated $[BMIM]^+$ cation; all less than 2.5 ppm and in most cases even less than 1 ppm.

The chemical shift differences of the C(4,5)-H protons for different anions are also significant, and these move upfield with the halide anion changing from Cl^- to I^-, suggesting that these hydrogen atoms also participate in hydrogen bonding with the anions, albeit to a lesser extent. From the DFT calculations these chemical shifts move from 7.2 ppm for the $[BMIM]^+$ cation to 6.7, 6.5, and 6.6 ppm for the [BMIM]BF_4, [BMIM]Br, and [BMIM]Cl ion-pairs, respectively. Thus, for these C(4,5)-H protons the ion-pair models are only useful to show that the induced changes are significantly smaller (~0.5 ppm) than for the C(2)-H protons, but fail to follow the experimental observations between the different anions. For the butyl chain of $[BMIM]^+$, starting from the C(7)-H protons, the chemical shift decreases quickly to ~4 ppm, thereafter it decreases monotonically as a function of the distance of the studied proton from the imidazolium ring. From the DFT calculations for [BMIM]Cl and [BMIM]Br chemical shifts of C(7)-H protons are found at 3.9 and 4.2 ppm, respectively. For [BMIM]BF_4, one of the proton attached to C(7) physically closer to the BF_4 anion has a chemical shift of 4.6 ppm, while the other C(7)-H proton has a value of 3.6 ppm. The observed upfield shift from C(7)-H to C(10)-H, also found in the DFT calculations for the halide ILs, is explained by the weakening of the inductive effect due to the increasing distance from the imidazolium ring, which also accounts for the big change from C(2)-H and C(4,5)-H to the rest of the protons.

In detail, the chemical shifts of [BMIM]BF_4 are clearly distinguishable from those of the halide based ILs, especially the much smaller shifts for C(2,4,5)-H is noticeable, confirming the hydrogen bonding is much weaker as compared to the halide salts. In addition, the chemical shifts are also not much different between C(2)-H and C(4,5)-H, suggesting a less specific hydrogen bonding. The DFT data support these observations with shifts of 10.0, 6.7,

and 6.7 ppm, for C(2,4,5)-H respectively, especially the C(2)-H chemical shift being much smaller than for the halide ILs.

At last, we also note that the order of the chemical shifts is reversed for the hydrogen atoms in the butyl chain for [BMIM]BF_4 (inset of Fig. 4), such that they are shifted more in the downfield region, as compared to the corresponding protons in the halide based ILs. We propose the following structure to account for this change; the BF_4^- anion is larger than the halide anions, thus introduces more free space in the bulk, and thereby more likeliness of the butyl chain to approach this anion. This results in the butyl-chain hydrogen atoms of [BMIM]BF_4 being relatively more downfield-shifted, presumably due to weak hydrogen bonding interactions with the BF_4^- anion.

3.3. Aqueous mixtures of ionic liquids: IR spectra

To unveil the microscopic structure of ILs we investigated IL/water mixtures. Our ILs are all fully miscible with water, and changing the concentration is an ingenious way to change the distance between anions and cations gradually, until they are remotely separated in very dilute solutions. The changes in the IR and NMR spectra at different concentrations will reflect these detailed structural changes and the differences between the ILs can be inferred.

The IR spectra of binary mixtures of [BMIM]X/water at different IL concentrations are shown in Fig. 5. In this experiment, D_2O was used instead of H_2O in order to avoid overlap between the C-H and O-H stretching bands in the [BMIM]X/water system. With the addition of water to [BMIM]X, the changes in the 2800 — 3000 cm^{-1} range were relatively minor for all the samples, but the absorption bands above 3000 cm^{-1} are blue-shifted significantly with dilution for [BMIM]Cl, [BMIM]Br and [BMIM]I. In stark contrast the spectra for [BMIM]BF_4/water mixtures did not change much upon dilution. At the lowest concentration (0.024 molar fraction, the lowest graphs in Fig. 5), all the spectra resemble each other, irrespective of anion, indicating the anions are quite far from the cations, and the IR spectra would represent

isolated $[BMIM]^+$ cations in water.

The large blue-shift of the bands above 3000 cm^{-1} for the aqueous mixtures is due to the weakening or breaking of the hydrogen bond between the protons in the imidazolium ring and the anion. The strength of hydrogen bonding is known to correlate with the amount of red-shift of the stretch vibration mode of the hydrogen participating in the bonding[77]. Thus, the large changes observed for halide based ILs indicate that the hydrogen bonding between the $[BMIM]^+$ cation and the halide anions is initially strong and specific, but decreases quickly upon dilution. As the peak positions of the dilute mixtures of these ILs are finally all similar to those of the $[BMIM]BF_4$ IL (see Fig. 5), the amount of blue-shift from pure ILs to very dilute mixtures is as much as ~100 cm^{-1} for C(2)-H of the [BMIM]Cl, slightly less for [BMIM]Br and [BMIM]I (or for C(4,5)-H), but still quite significant.

By contrast, the spectra of $[BMIM]BF_4$ /water mixtures (Fig. 5(d)) above 3000 cm^{-1} hardly changed with concentration throughout the range except the small overall peak shift. This indicates the environment provided by BF_4^- close to $[BMIM]^+$ for pure ILs is not too much different from $[BMIM]^+$ with no nearby anions, but surrounded by water molecules. This spectral feature thus strongly suggests that BF_4^- is not forming specific hydrogen bonding with the cation. In consistence with our IR experimental results, IR and large angle X-ray scattering (LAXS) experiments from other reports support weak and non-specific interaction between cation and anion in $[BMIM]BF_4$[44,45]. The interaction between the cation and anion was also found to be very weak and nonspecific in $[EMIM]BF_4/CD_2Cl_2$ mixtures[43].

Upon close inspection, slight blue-shift at higher D_2O concentration is observed for the bands corresponding to the butyl chains of the ILs, as reported for aqueous solutions of $[BMIM][BF_4]$[44]. The blue-shift of the C-H vibrational modes of alkyl chain in organic molecules in water mixtures has been reported earlier[78,79]. These peak shifts suggest that the halide anions also have hydrogen bonding with the protons in the butyl chain, even if weak and transient. The possibility of weak C-H···O hydrogen bonding was also suggested by *ab*

initio calculations[80].

A very similar picture emerged from the DFT calculations using the ion-pair models and C-PCM implicit solvation to mimic aqueous solutions. For [BMIM]Cl, that showed the largest peak shift upon dilution, the C(2)-H band shifted from 2746 cm^{-1} (in vacuum, see Table 2) to 3171 cm^{-1} (C-PCM), while for [BMIM]Br, the shift was less; from 2847 cm^{-1} to 3172 cm^{-1}. While the exact amount of shift is less important, the major observation is that for both ILs the implicit solvation renders a complete isolation of the cation from the anion – as all the frequencies for the cation ring C(2)-H band vibrations become independent of the IL anion. Thus, the observation of the similar spectra in Fig. 5 for the lowest halide IL concentrations is strongly supported by the DFT calculations. For [BMIM]BF_4, C-PCM calculation yields C(2)-H bands at 3171 cm^{-1}, further supporting the complete dissociation of the IL into cations and anions.

3.4 Aqueous mixtures of ionic liquids: NMR chemical shifts

1H NMR measurements were performed for D_2O/IL mixtures at different concentrations. The magnitude and nature of the chemical shift (δ) of the protons as a function of IL concentration reflect the change of the environment; anions gradually replaced by D_2O. With its high dielectric constant, water is a very effective medium to reduce the Coulombic interaction between the cations and anions in a controllable way by changing its concentration in the mixture[44]. The chemical shifts of hydrogen atoms with increasing ILs concentration are plotted in Fig. 6. For [BMIM]X (X = Cl^-, Br^-, I^-), the chemical shifts of C(2)-H, C(4)-H and C(5)-H undergo significant changes to an upfield position with decreasing IL concentration, and finally they all merge into the same value at very dilute concentrations, suggesting the cation and anion to be completely dissociated. This change in the chemical shift can be visualized as a gradual withdrawal of the anion (hydrogen-bonding acceptor) from these protons with a decreasing IL concentration. For C(4,5)-H of [BMIM]I, a brief downfield shift is seen (Fig. 6(b) and (c), green lines) at IL concentrations lower than ~ 0.1 mf. As can be

seen in Figs. 6(a), (b) and (c), the imidazolium ring protons in [BMIM]Cl are more downfield shifted than for [BMIM]I and [BMIM]Br, reflecting the strongest electronegativity of Cl^-.

This can be further corroborated by comparing the results of the DFT calculations for each ion-pair (and for the $[BMIM]^+$ cation) between the gas phase and water phase (C-PCM model) calculations. Using the isolated cation model, the vacuum and the C-PCM results should ideally not differ, thus serving as an internal reliability verification for the DFT computations; reassuringly the differences obtained are ~0.1 ppm or less. For the halide IL there are indeed huge changes occurring for the C(2)-H protons from the ion pairs in gas phase to those in water; for [BMIM]Cl from 14.8 to 8.3 ppm and for [BMIM]Br from 14.5 to 8.4 ppm. The shifts of the C(2)-H protons become almost identical for [BMIM]Cl and [BMIM]Br when they are "solvated", and much closer to the shift obtained for the "solvated" $[BMIM]^+$ cation of 7.7 ppm (thus only a 0.7 ppm difference). The large change between gas phase and continuum can also be visualized for the [BMIM]Cl ion-pair from the optimized geometries in Figs. 7(a) and (b), for the gas phase and for the solvated structure, respectively.

In contrast, the chemical shifts for $[BMIM]BF_4$ showed little change, which is also consistent with the IR spectra in Fig. 5(d), where the peak positions hardly changed with concentration. This indicates that the environment of all three protons do not undergo much change upon decreasing $[BMIM]BF_4$ concentration. In the DFT calculations the very same chemical shift for the C(2,4,5)-H protons (8.3, 7.6, and 7.6 ppm) is obtained as for the other ILs upon solvation, which further supports the loss of hydrogen bonding for the halide based ILs.

From this, we propose that the BF_4^- anion is positioned at/around the top of the imidazolium ring for pure $[BMIM]BF_4$ such that it cannot form any specific hydrogen bonding, as also suggested by previous studies and supported by the optimized configuration from DFT calculations as shown in Fig 7(c)[57,66,81] . With this weaker interaction between BF_4^- and C-H, the BF_4^- and the imidazolium cation seem and behave almost like separate entities. This can also explain why the chemical shifts of C(2)-H, C(4)-H and C(5)-H do not vary significantly

with decreasing [BMIM]BF_4 concentration (pink lines in Figs.6(a)-(c)). Due to this weak interaction, the C(2)-H, C(4)-H and C(5)-H peaks in IR spectra (Fig. 1) are more blue-shifted compared with [BMIM]X (X = Cl^-, Br^-, I^-). As for the relative position of BF_4^- *vs*. $[BMIM]^+$, previous reports also support our proposition[57,69,82].

To further investigate the relative position of the anions vs. the $[BMIM]^+$ imidazolium ring, we show in Fig. 8 and 9 an alignment of the chemical shifts values at infinite dilutions for different protons to a common zero value. Using these plots we find that for [BMIM]Cl, [BMIM]Br and [BMIM]I, C(2)-H is more downfield-shifted than C(4,5)-H (Figs. 8(a), (b), and (c)), indicating that the former protons are subject to a larger influence with increasing IL concentration. Again, this can be attributed to a stronger hydrogen bonding ability, and C(2)-H···anion interactions preferred over C(4,5)-H···anion interactions[41,83]. The chemical shifts all go upfield by dilution (except for a brief downfield shift for [BMIM]Br and [BMIM]I at very dilute concentrations lower than 0.1 mf, blue and red lines in Fig. 8(c)) for the halide based ILs.

In contrast to [BMIM]X (X = Cl^-, Br^-, I^-), the C(2)-H of [BMIM]BF_4 is upfield-shifted with increasing IL concentration (Fig. 8(d)), albeit only by a small amount. We propose that this is due to electron-rich BF_4^- ions shielding the imidazolium ring hydrogen atoms (C(2)-H, C(4)-H, C(5)-H) by being located around the top of the imidazolium rings, while the specific interaction between BF_4^- and C(2)-H is always very weak. Thus, by interpreting the outcomes from Figs. 5, 6 and 8, we propose that BF_4^- anion is positioned around the top of the imidazolium ring (Fig. 7(c)), and presumably closer to the C(4,5)-H. The chemical shifts from the DFT calculations are 6.7 ppm for the C(4,5)-H protons, and 10.0 ppm for the C(2)-H, qualitatively supporting the experimental results in Fig. 8(d).

In Fig. 9, the relative chemical shifts for the protons in the methyl group of the imidazolium ring and those in the butyl group are shown. With an increasing IL concentration a gradual upfield shift due to intermolecular effect would generally be expected, which is indeed shown

representatively in C(9)-H and C(10)-H for [BMIM]I and [BMIM]BF_4 (pink and green lines in Figs. 9(c) and (d)). This upfield shift is less prominent and even changes quickly to strong downfield shift for [BMIM]Cl and [BMIM]Br, especially for protons relatively closer to the imidazolium ring (see e.g. red and black lines in Figs. 9(a) and (b)). This indicates that hydrogen bonding between these protons and the halide anions (Cl^- and Br^-) gives rise to downfield shifts which overcome the intermolecular effect and results in a net downfield shift with increasing IL concentration.

As for [BMIM]BF_4 in Fig. 9(d), the chemical shift changes little with concentration, indicating the weaker interaction between BF_4^- and the protons in the butyl group overall. In detail, the chemical shift curves for C(6)-H and C(7)-H overlap for [BMIM]X (X = Cl^-, Br^-, I^-) (Figs. 9(a), (b), and (c)) suggesting the chemical environments of C(6)-H and C(7)-H are similar for these ILs. In contrast, for [BMIM]BF_4 the curves of C(6)-H and C(7)-H are separated (Fig. 9(d), black and red lines), suggesting slightly different environments for these protons.

3.5 H-D exchange of the C(2)-H in D_2O/IL mixture

As the C(2)-H is known to be the most acidic hydrogen of the imidazolium cation, its deuterium substitution rate in D_2O will be influenced by the hydrogen bonding strength within the IL. As shown in Fig. 10, the H(2) NMR peaks decrease at different rates depending on the size of halide anion, and for [BMIM]Cl decreases quickly after 21 h. After 3 days, the peak area ratios between H(2) and H(4) are 0.1, 0.14, 0.21 for [BMIM]Cl, [BMIM]Br and [BMIM]I, respectively. (In contrast, C(2)-H was completely deuterated after 20 hours for [BMIM]I in our previous work[66], likely accomplished by virtue of a ten-times lower IL concentration (0.01 mole fraction).

The deuterium exchange further confirms the hydrogen bonding strength to follow the order: C(2)-H···Cl > C(2)-H···Br > C(2)-H···I, as it weakens the C(2)-H bond and promotes

deuteration. In stark contrast, there is no exchange reaction at all for [BMIM]BF_4[66], and thus we infer also from this result no specific hydrogen bonding to promote the deuterium exchange to occur. We have proposed that BF_4^- is located out of the imidazolium ring plane, and is not forming specific hydrogen bonding with C(2)-H. The much smaller change for C(2)-H of [BMIM]BF_4 in the IR spectrum (Fig. 5(d)) and the NMR spectrum (Fig. 6(a)) upon dilution, and no H-D exchange in C(2)-H all support this proposition. Quantum chemical calculations show that positive charges are distributed over the imidazolium ring. Thus it can be imagined that the negative charges distributed over 4 fluoride atoms at the vertices of the tetrahedral BF_4^- favor this on-top position in terms of Coulomb attraction with the imidazolium cation.

4. Conclusions

We have investigated the bulk structures of [BMIM]X (X= Cl^-, Br^-, I^-) and [BMIM]BF_4 by IR and NMR spectra, all supported by DFT calculations. With a decreased halide anion size, the ν(C(2)-H) peak is more red-shifted in the IR spectrum, and the chemical shift of the C(2)-H proton moved further downfield in the NMR spectrum, which both suggest that the hydrogen bonding is stronger for C(2)-H with a smaller halide anion. The H-D exchange rates also confirm the hydrogen bonding strength to follow the order: C(2)-H···Cl > C(2)-H···Br > C(2)-H···I. Quite different from [BMIM]X (X= Cl^-, Br^-, I^-), the IR and NMR spectra in the imidazolium ring region of [BMIM]BF_4 did not change appreciably with concentration in our aqueous solution systems. This can be ascribed to a different relative position of the BF_4^- anion with respect to the $[BMIM]^+$ imidazolium ring and a different nature of the anion-cation interaction. Halide anions are expected to be in the imidazolium ring plane and close to the C(2)-H hydrogen, as indeed obtained as stable geometries for the DFT ion-pair model calculations, while BF_4^- is believed to be located above the imidazolium ring and thus farther away from the C(2)-H hydrogen. The joint observations of a much smaller vibrational shift for C(2)-H of [BMIM]BF_4 in the IR spectrum (Fig. 5(d)), the much smaller chemical shifts in the NMR spectrum (Fig. 6(a)) for this proton upon dilution, and the lack of H-D exchange for

the C(2)-H group, all support this particular IL to have weak hydrogen bonding. This structural difference between the ionic liquids depending upon the anions type will work as a key element to build further the structure-property relation of ionic liquids.

Acknowledgements

This work was supported by the National Research Foundation (NRF) grant funded by the Korea Government (MEST) No. 2011-0017435 and No. 2011-0031496. PJ and BA gratefully acknowledge the Swedish Research Council (VR) (dnr 2009-3082) for financial support.

REFERENCES

(1) Rogers, R. D.; Seddon, K. R. *Science* **2003**, *302*, 792–3.

(2) Welton, T. *Chem. Rev.* **1999**, *99*, 2071–2084.

(3) Albinet, A.; Papaiconomou, N.; Estager, J.; Suptil, J.; Draye, M.; Besombes, J.-L. *Anal. Bioanal. Chem.* **2010**, *396*, 857–64.

(4) Wu, W.; Han, B.; Gao, H.; Liu, Z.; Jiang, T.; Huang, J. *Angew. Chem. Int. Ed.* **2004**, *43*, 2415–7.

(5) Zhao, H.; Yu, N.; Ding, Y.; Tan, R.; Liu, C.; Yin, D.; Qiu, H.; Yin, D. *Micropor. Mesopor. Mater.* **2010**, *136*, 10–17.

(6) Akai, N.; Kawai, A.; Shibuya, K. *J. Phys. Chem. A* **2010**, *114*, 12662–6.

(7) Chang, T. M.; Dang, L. X.; Devanathan, R.; Dupuis, M. *J. Phys. Chem. A* **2010**, *114*, 12764–74.

(8) Sarangi, S. S.; Zhao, W.; Müller-Plathe, F.; Balasubramanian, S. *ChemPhysChem* **2010**, *11*, 2001–10.

(9) Gordon, P. G.; Brouwer, D. H.; Ripmeester, J. A. *ChemPhysChem* **2010**, *11*, 260–8.

(10) Cholico-Gonzalez, D.; Avila-Rodriguez, M.; Reyes-Aguilera, J. A.; Cote, G.; Chagnes, A. *J. Mol. Liq.* **2012**, *169*, 27–32.

(11) Cholico-Gonzalez, D.; Avila-Rodriguez, M.; Cote, G.; Chagnes, A. *J. Mol. Liq.* **2013**, *187*, 165–170.

(12) Kempter, V.; Kirchner, B. *J. Mol. Struct.* **2010**, *972*, 22–34.

(13) Tsuzuki, S.; Tokuda, H.; Hayamizu, K.; Watanabe, M. *J. Phys. Chem. B* **2005**, *109*, 16474–81.

(14) López-Martin, I.; Burello, E.; Davey, P. N.; Seddon, K. R.; Rothenberg, G. *ChemPhysChem* **2007**, *8*, 690–5.

(15) Singh, T.; Kumar, A. *J. Phys. Chem. B* **2007**, *111*, 7843–51.

(16) Triolo, A.; Russina, O.; Bleif, H.-J.; Di Cola, E. *J. Phys. Chem. B* **2007**, *111*, 4641–4.

(17) Atkin, R.; Warr, G. G. *J. Phys. Chem. B* **2008**, *112*, 4164–6.

(18) Fujii, K.; Kanzaki, R.; Takamuku, T.; Kameda, Y.; Kohara, S.; Kanakubo, M.; Shibayama, M.; Ishiguro, S.; Umebayashi, Y. *J. Chem. Phys.* **2011**, *135*, 244502.

(19) Canongia Lopes, J. N. A.; Pádua, A. A. H. *J. Phys. Chem. B* **2006**, *110*, 3330–5.

(20) Wang, Y.; Voth, G. A. *J. Am. Chem. Soc.* **2005**, *127*, 12192–3.

(21) Xiao, D.; Rajian, J. R.; Li, S.; Bartsch, R. A.; Quitevis, E. L. *J. Phys. Chem. B* **2006**, *110*, 16174–8.

(22) Jun, H.; Ouchi, Y.; Kim, D. *J. Mol .Liq.* **2013**, *179*, 54–59.

(23) Koeberg, M.; Wu, C.-C.; Kim, D.; Bonn, M. *Chem. Phys. Lett.* **2007**, *439*, 60–64.

(24) Hunt, P. A. *J. Phys. Chem. B* **2007**, *111*, 4844–53.

(25) Fumino, K.; Peppel, T.; Geppert-Rybczyńska, M.; Zaitsau, D. H.; Lehmann, J. K.; Verevkin, S. P.; Köckerling, M.; Ludwig, R. *Phys. Chem. Chem. Phys.* **2011**, *13*, 14064–75.

(26) Roth, C.; Peppel, T.; Fumino, K.; Köckerling, M.; Ludwig, R. *Angew. Chem. Int. Ed. Engl.* **2010**, *49*, 10221–4.

(27) Gao, Y.; Zhang, L.; Wang, Y.; Li, H. *J. Phys. Chem. B* **2010**, *114*, 2828–33.

(28) Dong, K.; Zhang, S.; Wang, D.; Yao, X. *J. Phys. Chem. A* **2006**, *110*, 9775–82.

(29) Fumino, K.; Wulf, A.; Ludwig, R. *Phys. Chem. Chem. Phys.* **2009**, *11*, 8790–4.

(30) Wulf, A.; Fumino, K.; Ludwig, R. *Angew. Chem. Int. Ed. Engl.* **2010**, *49*, 449–53.

(31) Lassègues, J.-C.; Grondin, J.; Cavagnat, D.; Johansson, P. *J. Phys. Chem. A* **2010**, *114*, 687–688.

(32) Grondin, J.; Lassègues, J.-C.; Cavagnat, D.; Buffeteau, T.; Johansson, P.; Holomb, R. *J. Raman Spectrosc.* **2011**, *42*, 733–743.

(33) Lassègues, J.-C.; Grondin, J.; Cavagnat, D.; Johansson, P. *J. Phys. Chem. A* **2009**, *113*, 6419–21.

(34) Shukla, M.; Srivastava, N.; Saha, S. *J. Mol. Struct.* **2010**, *975*, 349–356.

(35) Chen, S.; Vijayaraghavan, R.; MacFarlane, D. R.; Izgorodina, E. I. *J. Phys. Chem. B* **2013**, *117*, 3186–97.

(36) Popolo, M. G. Del; Lynden-bell, R. M.; Kohanoff, J. *J. Phys. Chem. B* **2005**, 5895–5902.

(37) Bhargava, B. L.; Balasubramanian, S. *Chem. Phys. Lett.* **2006**, *417*, 486–491.

(38) Elaiwi, A.; Hitchcock, P. B.; Seddon, K. R.; Srinivasan, N.; Tan, Y.; Weltonc, T.; Zoraa, J. A.; Building, D. K.; Sag, B. B. T. *J. Chem. Soc. Dalt. Trans.* **1995**, 3467.

(39) Avent, A. G.; Chaloner, P. A.; Day, M. P.; Seddon, K. R.; Welton, T. *J. Chem. Soc. Dalt. Trans.* **1994**, 3405.

(40) Mele, A.; Tran, C. D.; De Paoli Lacerda, S. H. *Angew. Chem. Int. Ed.* **2003**, *42*, 4364–6.

(41) Huang, J.-F.; Chen, P.-Y.; Sun, I.-W.; Wang, S. P. *Inorg. Chim. Acta.* **2001**, *320*, 7–11.

(42) Zhang, L.; Xu, Z.; Wang, Y.; Li, H. *J. Phys. Chem. B* **2008**, *112*, 6411–9.

(43) Katsyuba, A.; Dyson, P. J.; Vandyukova, E. E.; Chernova, A. V; Vidis, A. *Helv. Chim. Acta* **2004**, *87*, 2556–2565.

(44) Jeon, Y.; Sung, J.; Kim, D.; Seo, C.; Cheong, H.; Ouchi, Y.; Ozawa, R.; Hamaguchi, H. *J. Phys. Chem. B* **2008**, *112*, 923–8.

(45) Takamuku, T.; Kyoshoin, Y.; Shimomura, T.; Kittaka, S.; Yamaguchi, T. *J. Phys. Chem. B* **2009**, *113*, 10817–24.

(46) Zhang, L.; Wang, Y.; Xu, Z.; Li, H. *J. Phys. Chem. B* **2009**, *113*, 5978–84.

(47) Zheng, Y.-Z.; Wang, N.-N.; Luo, J.-J.; Zhou, Y.; Yu, Z.-W. *Phys. Chem. Chem. Phys.* **2013**, *15*, 18055–64.

(48) Wang, N.-N.; Zhang, Q.-G.; Wu, F.-G.; Li, Q.-Z.; Yu, Z.-W. *J. Phys. Chem. B* **2010**, *114*, 8689–700.

(49) Zhang, Q.-G.; Wang, N.-N.; Yu, Z.-W. *J. Phys. Chem. B* **2010**, *114*, 4747–54.

(50) Chen, Y.; Cao, Y.; Sun, X.; Mu, T. *J. Mol. Liq.* **2014**, *190*, 151–158.

(51) Dominguez-Vidal, A.; Kaun, N.; Ayora-Cañada, M. J.; Lendl, B. *J. Phys. Chem. B* **2007**, *111*, 4446–52.

(52) Asaki, M. L. T.; Redondo, A.; Zawodzinski, T. A.; Taylor, A. J. *J. Chem. Phys. 116*, 10377.

(53) Bardak, F.; Xiao, D.; Hines, L. G.; Son, P.; Bartsch, R. A.; Quitevis, E. L.; Yang, P.; Voth, G. A. *ChemPhysChem* **2012**, *13*, 1687–1700.

(54) Chagnes, A.; Allouchi, H.; Carre, B.; Lemordant, D. *Solid State Ionics* **2005**, *176*, 1419–1427.

(55) Moreno, M.; Castiglione, F.; Mele, A.; Pasqui, C.; Raos, G. *J. Phys. Chem. B* **2008**, *112*, 7826–36.

(56) Porter, A. R.; Liem, S. Y.; Popelier, P. L. A. *Phys. Chem. Chem. Phys.* **2008**, *10*, 4240–8.

(57) Holomb, R.; Martinelli, A.; Albinsson, I.; Lassègues, J. C.; Johansson, P.; Jacobsson, P. *J. Raman Spectrosc.* **2008**, *39*, 793–805.

(58) Zhang, L.; Wang, Y.; Xu, Z.; Li, H. *J. Phys. Chem. B* **2009**, *113*, 5978–84.

(59) Fumino, K.; Wulf, A.; Ludwig, R. *Angew. Chem. Int. Ed.* **2008**, *47*, 8731–4.

(60) Zhu, X.; Gao, Y.; Zhang, L.; Li, H. *J. Mol. Liq.* **2014**, *190*, 174–177.

(61) Cesare Marincola, F.; Piras, C.; Russina, O.; Gontrani, L.; Saba, G.; Lai, A. *ChemPhysChem* **2012**, *13*, 1339–46.

(62) Tokuda, H.; Hayamizu, K.; Ishii, K.; Susan, M. A. B. H.; Watanabe, M. *J. Phys. Chem. B* **2005**, *109*, 6103–10.

(63) Tokuda, H.; Hayamizu, K.; Ishii, K.; Susan, M. A. B. H.; Watanabe, M. *J. Phys. Chem. B* **2004**, *108*, 16593–16600.

(64) Noda, A.; Hayamizu, K.; Watanabe, M. *J. Phys. Chem. B* **2001**, *105*, 4603–4610.

(65) Nakakoshi, M.; Ishihara, S.; Utsumi, H.; Seki, H.; Koga, Y.; Nishikawa, K. *Chem. Phys. Lett.* **2006**, *427*, 87–90.

(66) Jeon, Y.; Sung, J.; Seo, C.; Lim, H.; Cheong, H.; Kang, M.; Moon, B.; Ouchi, Y.; Kim, D. *J. Phys. Chem. B* **2008**, *112*, 4735–40.

(67) Barone, V.; Cossi, M. *J. Phys. Chem. A* **1998**, *102*, 1995–2001.

(68) M. J. Frisch, G. W. Trucks, H. B. Schlegel, G. E. Scuseria, M. A. Robb, J. R. Cheeseman, G. Scalmani, V. Barone, B. Mennucci, G. A. Petersson, H. Nakatsuji, M. Caricato, X. Li, H. P. Hratchian, A. F. Izmaylov, J. Bloino, G. Zheng, J. L. Sonnenberg, M. H.; Fox, D. J. Gaussian 09, Revision A.1 **2009**.

(69) Katsyuba, S. A.; Zvereva, E. E.; Vidis, A.; Dyson, P. J. *J. Phys. Chem. A* **2007**, *111*, 352–70.

(70) Berg, R. W.; Deetlefs, M.; Seddon, K. R.; Shim, I.; Thompson, J. M. *J. Phys. Chem. B* **2005**, *109*, 19018–25.

(71) Brubach, J.-B.; Mermet, A.; Filabozzi, A.; Gerschel, A.; Lairez, D.; Krafft, M. P.; Roy, P. *J. Phys. Chem. B* **2001**, *105*, 430–435.

(72) Dieter, K. M.; Dymek, C. J.; Heimer, N. E.; Rovang, J. W.; Wilkes, J. S. *J. Am. Chem. Soc.* **1988**, *110*, 2722–2726.

(73) Chang, H.-C.; Jiang, J.-C.; Tsai, W.-C.; Chen, G.-C.; Lin, S. H. *J. Phys. Chem. B* **2006**, *110*, 3302–7.

(74) Becker, E. D. *High Resolution NMR:Theory and Chemical Applications*; 3rd editio.; Academic Press: San Diego, 1999.

(75) Ebenso, E. E. *Mater. Chem. Phys.* **2003**, *79*, 58–70.

(76) Palomar, J.; Ferro, V. R.; Gilarranz, M. A.; Rodriguez, J. J. *J. Phys. Chem. B* **2007**, *111*, 168–80.

(77) Yokozeki, A.; Kasprzak, D. J.; Shiflett, M. B. *Phys. Chem. Chem. Phys.* **2007**, *9*, 5018–26.

(78) Mizuno, K.; Imafuji, S.; Ochi, T.; Ohta, T.; Maeda, S. *J. Phys. Chem. B* **2000**, *104*, 11001–11005.

(79) Mizuno, K.; Miyashita, Y.; Shindo, Y.; Ogawa, H. *J. Phys. Chem.* **1995**, *99*, 3225–3228.

(80) Gu, Y.; Kar, T.; Scheiner, S. *J. Am. Chem. Soc.* **1999**, 9411–9422.

(81) Holbrey, J. D.; Seddon, K. R. *J. Chem. Soc.,Dalt. Trans.* **1999**, 2133–2139.

(82) Liu, Z.; Huang, S.; Wang, W. *J. Phys. Chem. B* **2004**, *108*, 12978–12989.

(83) Wang, Y.; Li, H.; Han, S. *J. Phys. Chem. B* **2006**, *110*, 24646–51.

Table 1. Gaussian fitting values obtained from the IR absorption spectra (Fig. 2) for pure [BMIM]Cl, [BMIM]Br, [BMIM]I, and [BMIM]BF_4.

	[BMIM][BF_4]	[BMIM]I	[BMIM]Br	[BMIM]Cl
v_{ss}HC(4)C(5)H	3163	3018	3018	3137
v_{as}HC(4)C(5)H	3122	3078	3074	3057
vC2(H)	3114	3032	3020	3018
v_{as}(N)CH_3	3036	3019	3015	2995
v_{ss}(N)CH_3	2985	2981	2980	2078
$v_{as}CH_3$	2965	2956	2957	2957
$v_{FR}CH_3$	2938	2932	2934	2934
$v_{ss}CH_3$	2877	2870	2870	2870
$v_{as}CH_2$	2913	2906	2906	2907
$v_{ss}CH_2$	2856	2848	2844	2845

Table 2. IR frequencies and NMR chemical shifts from the DFT calculations.

	[BMIM]Cl		[BMIM]Br		[BMIM]BF_4		$[BMIM]^+$	
	vacuum	C-PCM	vacuum	C-PCM	vacuum	C-PCM	vacuum	C-PCM
	IR frequency (cm^{-1})							
ν(C(2)-H)	2746	3171	2847	3172	3250	3171	3284	3219
ν_{as}(C(4,5)-H)	3272	3189	3274	3188	3270	3188	3280	3232
ν_{ss}(C(4,5)-H)	3291	3206	3293	3206	3298	3206	3298	3250
	NMR chemical shift (ppm)							
C(2)-H	14.8	8.3	14.5	8.4	10	8.3	7.6	7.7
C(4,5)-H	6.6	7.6	6.5	7.6	6.7	7.6	7.2	7.3
C(4,5)-H	6.6	7.6	6.5	7.6	6.7	7.6	7.2	7.3

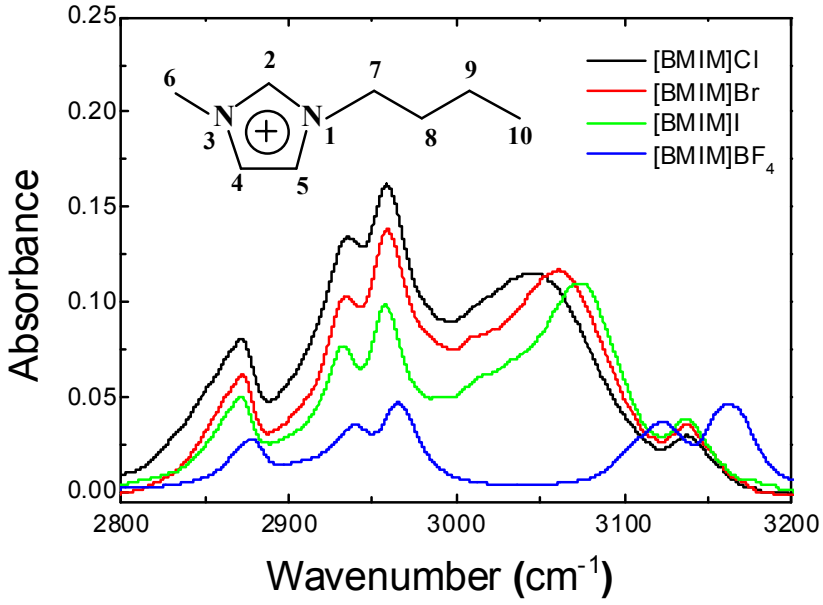

Figure 1. IR spectra of pure [BMIM]Cl, [BMIM]Br, [BMIM]I and [BMIM]BF_4 in the CH_x range. Inset shows the chemical structure of the 1-butyl-3-methyl imidazolium cation ($[BMIM]^+$).

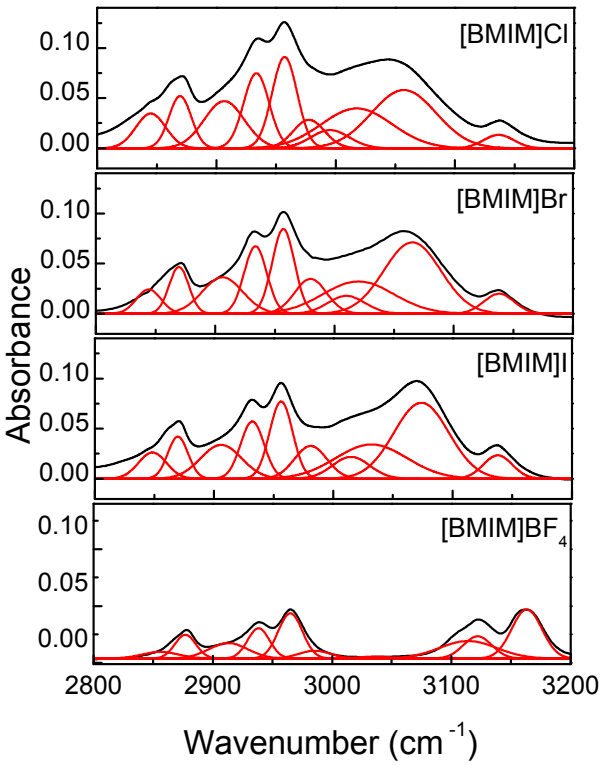

Figure 2. Deconvolution of the IR spectra in the CH_x range for pure [BMIM]Cl, [BMIM]Br, [BMIM]I, and [BMIM]BF_4.

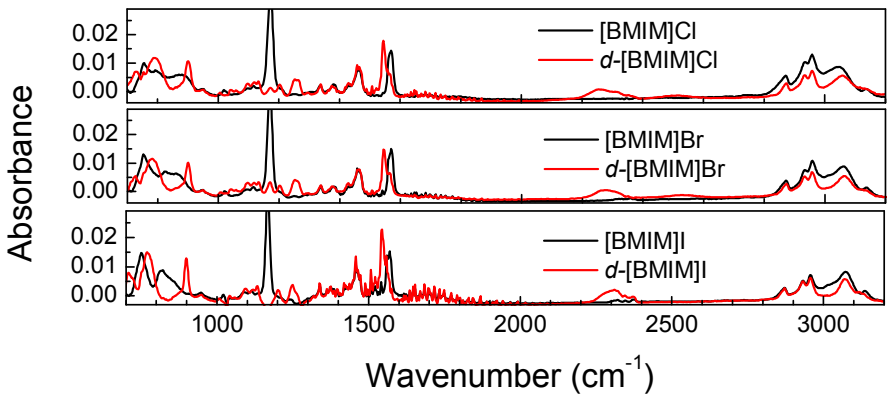

Figure 3. IR spectra of pure [BMIM]Cl, [BMIM]Br, [BMIM]I and their isotopic substituted d-[BMIM]Cl,

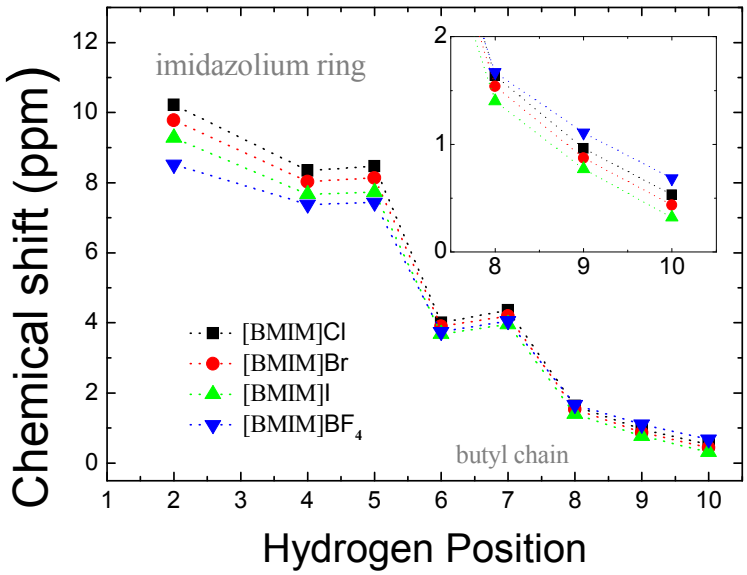

Figure 4. NMR chemical shifts of various protons (as labelled in Fig. 1) of imidazolium cations in pure ILs.

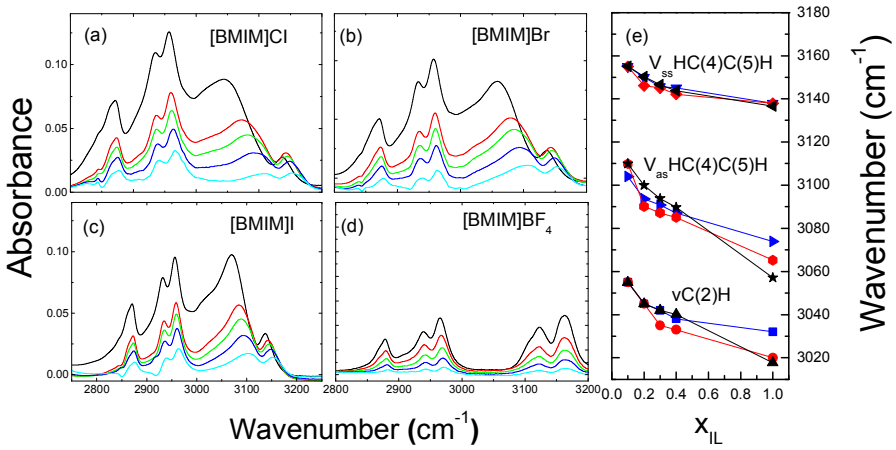

Figure 5. IR absorption spectra of [BMIM]X/D_2O. In (a), (b) and (c), from bottom to top, the molar fraction (mf) of ILs is 0.1, 0.2, 0.3, 0.4 and 1, respectively. In (d) [29], from bottom to top, the molar fraction (mf) of ILs is 0.024, 0.054, 0.12, 0.23 and 1. (e) peak positions of C(2)-H and C(4,5)-H vibrational modes vs. concentration (black: [BMIM]Cl, red: [BMIM]Br, blue: [BMIM]I)

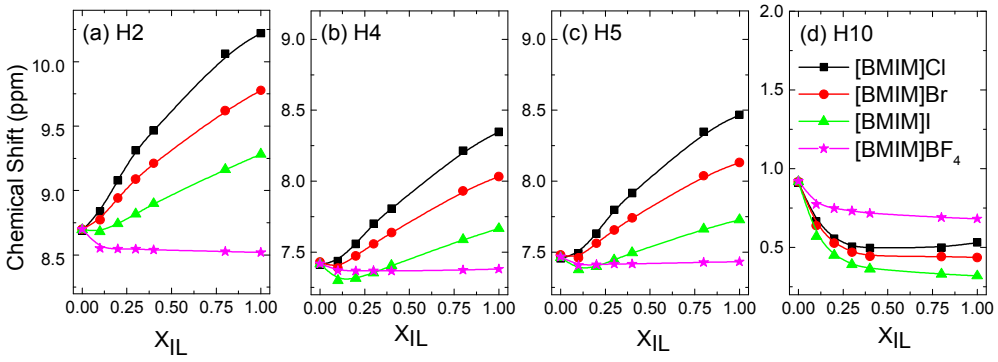

Figure 6. Chemical shift δ_{obsd} (ppm) of C(2,4,5,10)-H protons with increasing [BMIM]X (X= Cl^-, Br^-, I^-, BF_4^-) concentration in water.

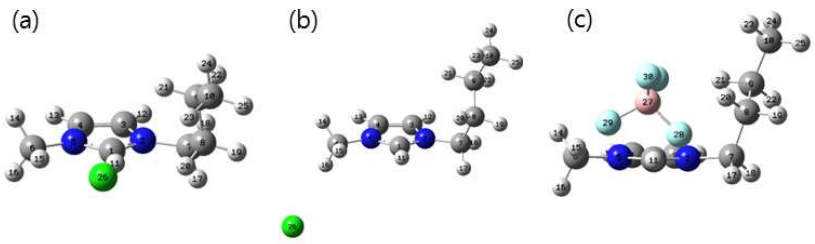

Figure 7: The optimized geometries, B3LYP/6-311+G*, of the [BMIM]X ion-pair with the cation in the GA conformation, in: (a) gas phase and (b) using the C-PCM continuum model with water as solvent X = Cl, (c) gas phase X = BF_4.

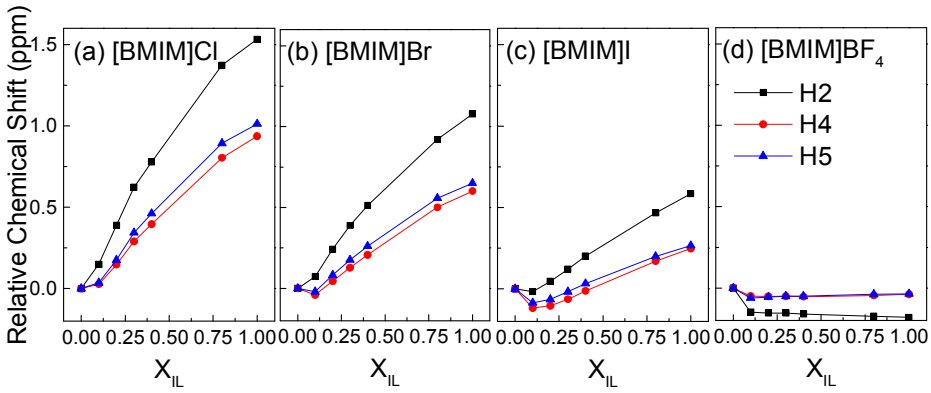

Figure 8. Normalized chemical shift δ_{obsd} (ppm) of protons in imidazolium ring with increasing [BMIM]X (X= Cl^-, Br^-, I^-, BF_4^-) concentration in water.

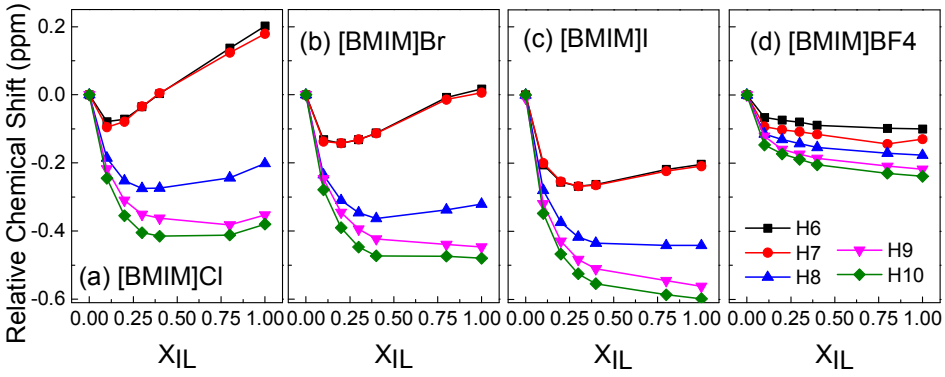

Figure 9. Normalized chemical shift δ_{obsd} (ppm) of protons in alkyl chain with increasing [BMIM]X (X= Cl^-, Br^-, I^-, BF_4^-) concentration in water.

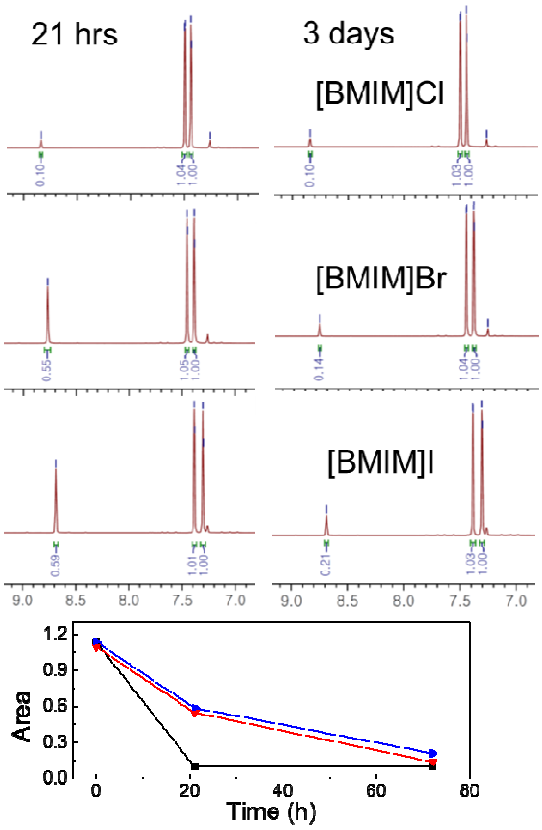

Figure 10. HNMR spectra of [BMIM]X (X= Cl^-, Br^-, I^-) in D_2O at 0.1 mole fraction: (upper left) after 21 h; (upper right) after 3 days. (below) C(2)-H peak area change vs. time concentration (black: [BMIM]Cl, red: [BMIM]Br, blue: [BMIM]I).